ELSEVIER

Physica C 353 (2001) 167–183

PHYSICA C

www.elsevier.nl/locate/physc

Structure and properties of (Sr,Ca)CuO_2–$BaCuO_2$ superlattices grown by pulsed laser interval deposition

Gertjan Koster [a,1], Karen Verbist [b,2], Guus Rijnders [a], Horst Rogalla [a], Gustaav van Tendeloo [b], Dave H.A. Blank [a,*]

[a] *MESA+ Research Institute and Low Temperature Division, Department of Applied Physics, University of Twente, P.O. Box 217, 7500 AE Enschede, Netherlands*

[b] *EMAT, University of Antwerp (RUCA), Antwerp, Belgium*

Received 19 November 1999; received in revised form 28 July 2000; accepted 1 November 2000

Abstract

We report on the preparation of $CuBa_2(Sr_xCa_{1-x})_nCu_{n-1}O_y$ compounds by fabrication of (Ba,Sr,Ca)CuO_2 superlattices with pulsed laser deposition (PLD). A technique called interval deposition is used to suppress multi-level or island growth resulting in high-quality superlattice structures. Both, the applicability of PLD to atomic engineering as well as the fabrication of artificial superconductors is demonstrated. The (Sr,Ca)CuO_2–$BaCuO_2$ superlattices are characterized by X-ray diffraction, high-resolution electron microscopy (HREM) and selected area electron diffraction. The superlattice period has been deduced from electron diffraction patterns and XRD measurements. For Sr containing films, the best growth behavior is observed and films with the highest degree of crystallinity are obtained, whereas superconductivity is only found in less crystalline, Ca containing films. Under some deposition conditions and depending on the amount of Ba containing layers in the superlattice, it was observed that the $BaCuO_2$ material is converted to $Ba_2CuO_{4-\delta}$. Image simulations to interpret the HREM contrast are performed.

Keywords: Perovskites; Epitaxy; Superlattices; Pulsed laser deposition; RHEED

1. Introduction

Almost all high-T_c superconducting oxide ceramics belong to the perovskite class of materials. This layered structure has invited people to intervene on an atomic level. In search for new superconducting compounds, in particular the cuprates, layer-by-layer or block-by-block thin film deposition techniques have become an interesting alternative to the traditional 'bulk' synthesis methods [1]. These techniques have been used to systematically investigate superconducting properties of atomically (or molecularly) engineered structures, i.e., superlattices of superconductors and insulators [2–7], other combinations [8–10] and 'known' structures with insertion of extra (up to eight)

* Corresponding author. Tel.: +31-53-489-3121; fax: +31-53-489-1099.

E-mail address: d.h.a.blank@tn.utwente.nl (D.H.A. Blank).

[1] Present address: Department of Applied Physics, Stanford University, Stanford, CA 94305, USA.

[2] Present address: Soft Imaging System GmbH, Hammerstr. 89, Münster, Germany.

0921-4534/01/$ - see front matter
PII: S0921-4534(00)01763-9

copper oxide planes [11–14]. Finally, similar techniques have been used to fabricate very thin barrier layers for Josephson junctions with a planar layout [11,15–17].

In the search for new superconducting compounds an often chosen strategy is to assume the so-called infinite-layer compound $ACuO_2$ and try to periodically insert some kind of the charge reservoir. The infinite-layer structure $ACuO_2$ ($A = Ba, Sr, Ca$) is an oxygen deficient perovskite structure, consisting of corner shared, square coordinated Cu(II), copper oxide planes, and alkaline(II) earth in the body center. In fact, many classification schemes of the known high-T_c cuprates are based on the infinite-layer or 'parent' structure [18,19]. It was first thought that the 'infinite-layer' compound has the simplest structure containing all the elements for high-T_c superconductivity. After the stabilization of tetragonal $Sr_{0.14}Ca_{0.86}CuO_2$ by Siegrist et al. in 1988 [20] numerous efforts to make this structure superconducting have lead to an abundance of new compounds.

Parallel to the synthesis of bulk infinite-layer compounds at high pressures, it became clear that the tetragonal phase for different film compositions could be epitaxially stabilized on different substrate materials using pulsed laser deposition (PLD) [21–28], RF magnetron sputtering [29–33], laser-molecular-beam epitaxy (laser-MBE) [34–38], molecular-beam epitaxy (MBE) [39] or other techniques [40,41].

Indeed, doped structures with some Sr^{2+} or Ca^{2+} replaced by Ln^{3+} (Ln = La, Nd), synthesized by several groups either in bulk [42–46] or thin film [47–51] with T_cs up to ~40 K, have the tetragonal structure. These materials are n-type or electron doped superconductors. However, in some reports the formation of foreign phases is observed depending on the doping level (e.g. [52]). Since the Meissner fraction for most of the n-type samples is rather small, the question remains whether the observed superconductivity should be ascribed to the infinite-layer structure itself.

Holes (p-type) are created in slightly alkaline earth deficient compositions with an infinite-layer structure and there have been several reports of critical temperatures up to 110 K [53]. However, the high critical temperatures were measured in samples containing a lot of ordered defect structures, as seen with high-resolution electron microscopy (HREM). This suggests that in fact these defects play an important role in the doping of the CuO_2 planes [54–57]. For a detailed discussion see for example the review article of Laguës et al. [58]. This observation has been explored extensively in, both, bulk material as well as thin films. For example, Feenstra et al. [59,60] show that periodical insertion of extra SrO layers, acting as defects, using thin film techniques, leads to either n-type or p-type conduction, depending on the post-anneal procedure.

Also substitution of smaller Ca^{2+} ($r = 0.112$ nm) by Sr^{2+} ($r = 0.126$ nm) or Ba^{2+} ($r = 0.142$ nm) in solid solutions of $BaCuO_2$, $SrCuO_2$ and $CaCuO_2$ led sometimes to higher T_cs [61,62]. Although initially incorporation of excess oxygen due to the difference in coordination number of Ba^{2+} compared to $(Sr,Ca)^{2+}$ was held responsible for the doping, also here different types of ordered defects were found.

For superlattices created by sequential deposition containing only $SrCuO_2$ and $CaCuO_2$ [63–65], no superconductivity was found. However, Norton et al. have demonstrated superconducting artificial layered structures with $BaCuO_2$ and $(Sr_{1-x},Ca_x)CuO_2$ by PLD [66], with a maximum T_c of ~70 K. The idea behind this is the fact that by periodically substituting layers with smaller cations by larger cations, extra oxygen may be incorporated in the latter acting as charge reservoirs. They only observed superconductivity in structures with more than one $BaCuO_2$ block. Later, Balestrino et al. found also superconductivity ($T_{c,max} \sim 80$ K) using the same method, however, only in case of superlattices with Ba and Ca [67], i.e., Sr containing structures showed no trace of superconductivity. This was attributed to Ba/Sr interdiffusion. Both groups verified the artificial periodicity of the as-grown films with XRD [68], after calibration of the growth rates of the individual constituents by thickness measurements: no in situ growth rate monitoring has been used and, more importantly, the growth mode has not been identified in these studies. Because these structures are very unstable, HREM analysis of these films,

using high-energy electrons, is extremely difficult. The relation of superconductivity and the structure is not clear yet, e.g., whether the relation found for the number of different layers with superconductivity [69] has a fundamental origin or is determined by the crystalline quality.

As a result of the efforts to explore the origin of superconductivity in infinite-layer materials, new superconducting families were identified, e.g., $Sr_{n+1}Cu_nO_{2n+1+\delta}$ [54], $Cu_zBa_2Ca_{n-1}Cu_nO_y$ [70] and the oxy-carbonates [71–75]. The highest critical temperature up to now for materials without heavy metals is reported for the $Ca_{0.5}Cu_{0.5}Ba_2Ca_{n-1}Cu_nO_y$ system in bulk [76,77] and is 126 K. Note that this is comparable to materials containing the highly toxic elements like thallium or mercury and, therefore, these materials are very attractive for application.

Here, the $CuBa_2(Sr,Ca)_{n-1}Cu_nO_y$ compound has been fabricated in thin film by sequential deposition of (smaller) Sr_{1-x}, Ca_x containing layers and (larger) Ba containing layers, in order to obtain layers with different functionalities (e.g., charge reservoir by incorporation of excess oxygen). Superlattices are fabricated by depositing sequentially $ACuO_2$ (A = Ba, Sr or Ca) from different targets, $BaCuO_2$ (BCO), $SrCuO_2$ (SCO), $Sr_{0.7}Ca_{0.3}CuO_2$ (SCCO) and $CaCuO_2$ (CCO), using the interval deposition technique. The structures have been analyzed with XRD and HREM and the morphology of the surface is monitored in situ with high-pressure reflective high energy electron diffraction RHEED and ex situ with AFM.

2. Experimental

The thin films were grown using the atomic layer-by-layer PLD system, including high-pressure RHEED, as described by Rijnders et al. [78]. The technical details were the following: Lambda Physik Compex 105 Excimer KrF laser (248 nm), energy density on the targets 1.5 J/cm^2, repetition rate of 1–10 Hz, target–substrate distance set at ~50 mm, oxygen pressure varied between 3 and 31 Pa. All targets used were sintered pellets. For the RHEED analysis, 35 keV electrons, STAIB Instrumente, were used with an incident angle of 1–2°. The diffraction pattern on the phosphor screen was monitored during growth by a CCD camera.

Special treated $SrTiO_3$ substrates have been used to ensure a single terminated surface, i.e., TiO_2 [79,80]. In some cases the surface termination was changed by deposition one monolayer of SrO.

For each succeeding layer in the artificial superlattices, the pulsed laser interval deposition method was used to suppress island growth [81]. To perform successfully interval deposition, one needs to know the number of laser pulses p_i to complete one unit-cell layer for each of the components i. Therefore, the following procedure was applied for the superlattices. First, the number of pulses needed for one unit-cell layer is estimated by counting the number of pulses completing one oscillation period during the deposition of each component at fixed deposition conditions. Note that in this case no interval deposition was used, but standard PLD, with a repetition rate of 1 Hz. If possible, this estimation is verified with X-ray reflectivity thickness measurements. In some cases, e.g., CCO, intensity oscillations could only be observed in the presence of an extra buffer layer.

Subsequently, the *interval* deposition technique is used to deposit stacks of layers where two unit-cell BCO layers (Balestrino et al. observed that the BCO is only stable when at least a double block is deposited [27,87,88]) are alternated with CCO, SCCO or SCO layers of different combinations and thickness (up to four tetragonal unit-cell layers). θ–2θ scans (X'pert diffractometer, Philips, The Netherlands, CuKα source) show satellite peaks, originating from the artificial superstructures, see for example Ref. [82]. The positions of these satellite peaks were used to confirm the deposition rate of each constituent. From the superlattice period

$$\Lambda = \frac{\lambda}{2|\sin\theta_{\pm1} - \sin\theta_0|} \tag{1}$$

of the subsequently deposited film and the average lattice parameter

$$\bar{c} = (n_1c_1 + n_2c_2)/(n_1 + n_2) \tag{2}$$

with λ the wavelength of the used radiation, $\theta_{\pm1}$ the angles of the first-order satellite peaks and n_i

the number of constituent layers with lattice parameter c_i, one can estimate p_i notifying that for an expected Λ, n_i have to be integers.

The HREM analyses were performed on a JEOL 4000EX operating at 400 and 376 kV. The point resolution of this instrument is 0.17 nm. The HREM sample preparation involves standard polishing and ion milling at low angle and low voltage. Samples with growth sequences of $[(Sr_{1-x},Ca_x)CuO_2)_a$–$(BaCuO_2)_b]_n$ and $n = 20$; $a = b = 4$, $n = 20$; $a = 2$; $b = 3$ and $n = 20$; $a = b = 2$ have been investigated by HREM.

The electrical properties of the superlattices were measured with the four-probe technique, inside a He cryostat.

3. Results and discussion

3.1. Deposition of constituents

To be able to fabricate superlattices in the (Ba,Sr,Ca)CuO_2 system, we first studied the growth of the individual constituents by standard PLD (repetation rate 1 Hz) on $SrTiO_3$. Fig. 1 shows the RHEED intensity changes of the specular reflection recorded during the deposition of CCO, SCO and BCO on $SrTiO_3$.

During the growth of the infinite-layer $ACuO_2$ on $SrTiO_3$ ($a_0 = 0.3905$ nm), the observed behavior strongly depends on the size of the alkaline earth ion A. The bulk lattice constants for tetragonal CCO and SCO are 0.3855 and 0.3926 nm, the values for the c-axis are 0.318 and 0.343 nm, respectively [26,61,83]. The lattice constants for thin films on $SrTiO_3$ tend to deviate a little from these values, possibly due to the underlying crystalline template of $SrTiO_3$, see below. No data exists for BCO, since the tetragonal structure is not stable in bulk.

Here, SCO was deposited on SrO terminated $SrTiO_3$ at a temperature of 550°C and oxygen pressure of 3 Pa. After an initial dip of the specular intensity, a stationary variation is observed. SCO (or SCCO) with a lattice constant comparable to the one of $SrTiO_3$ exhibits a layer-by-layer growth mode, as seen from the pronounced intensity oscillations in Fig. 1(a).

In contrast, for CCO a Stransky–Krastanov growth behavior, i.e., two unit-cell layers are stabilized by the substrate, as seen in Fig. 1(b) by the existence of two maxima, followed by an expo-

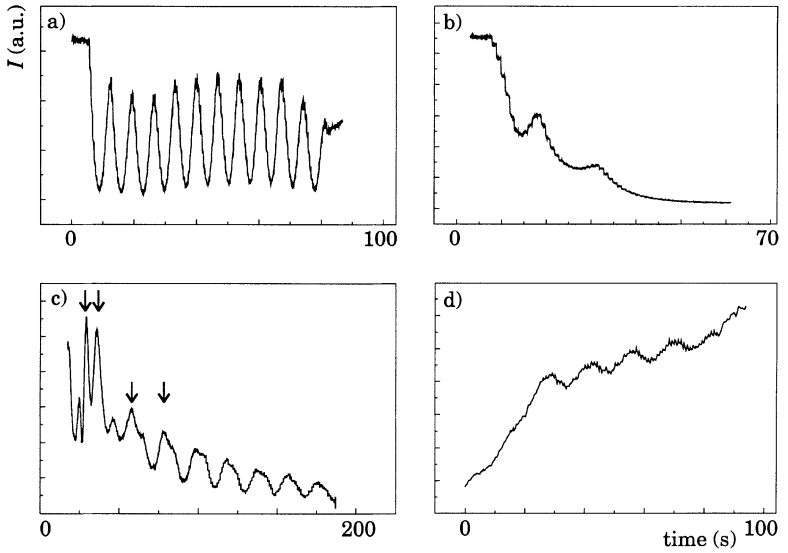

Fig. 1. RHEED intensity changes of the specular reflection recorded during deposition of (a) SCO, (b) CCO on $SrTiO_3$ and (c) BCO, (d) CCO on buffered $SrTiO_3$ (standard PLD; repetition rate 1 Hz).

nential decay. The small in-plane lattice constant, compared to $SrTiO_3$ and the relaxation of stress can explain this.

As mentioned before, the tetragonal BCO phase is not stable in bulk and it is only possible to grow in thin film form through the stabilizing effect of substrate. The tetragonal phase of BCO has been reported to be stable in thin film form up to thickness of 30 nm [84]. Due to the larger size of Ba^{2+} compared to Sr^{2+}, one expects considerable compressive stress in the BCO film that eventually will be released in thicker films. During deposition of BCO on SCO buffered $SrTiO_3$, a transition in the period of the intensity oscillations is observed, as indicated by the arrows in Fig. 1(c), which might indicate that the growing block, corresponding to the RHEED intensity variations, has been changed. The change during the growth of BCO, as clearly can be seen in the figure, might be explained by a phase transformation for thicker films. This behavior was observed both on a bare substrate as well as on substrates buffered, e.g., with SCO. Note, that Del Vecchio et al. proposed that BCO growth proceeds in double unit-cell blocks [88].

When a buffer layer of BCO is used prior to the deposition of CCO, see Fig. 1(d), the intensity increases and intensity oscillations are observed. The same behavior is observed during the growth of CCO on SCO buffered $SrTiO_3$. A better estimate can be made of the deposition rate in this case, since more periods can be taken into account.

In Fig. 2, the θ–2θ XRD data are given for the different constituents. From the (0 0 l) reflections marked in Fig. 2(a)–(c) by arrows, we determined the c-axis periods for CCO, SCCO, SCO and BCO to be 0.321, 0.341, 0.345 and 0.421 nm, respectively. These values are comparable to the ones found in literature for different deposition techniques. From the RHEED patterns we estimate that the in-plane lattice constants are comparable to $SrTiO_3$. Note that the value found for BCO is the one expected for the tetragonal phase, this in contradiction one should expect from the RHEED data. This supports the assumption of a more stable double tetragonal BCO block during deposition. Some very small peaks, marked with ? in Fig. 2(c), could not be identified as originating from a superstructure phase.

Although these results suggest that only for SCO and SCCO the RHEED intensity oscillations can be used for rate monitoring, the initial periods of both CCO and BCO have been used for a first estimation of their deposition rate.

3.2. Deposition of superlattices

In Fig. 3 typical RHEED patterns are shown observed after sequential deposition of a BCO layer (a) and a subsequent layer containing Ca and/or Sr (b). The pattern after deposition of BCO is always streaky and the intensity drops significantly. After subsequent deposition of the SCO, SCCO or CCO layer, the intensity increases again and usually a tendency to a transmission spotty-like pattern is observed, see Fig. 3(b). In Fig. 3(c) the profile, of the 'specular' streak after seven blocks of BCO/SCO, BCO/SCCO, BCO/CCO and

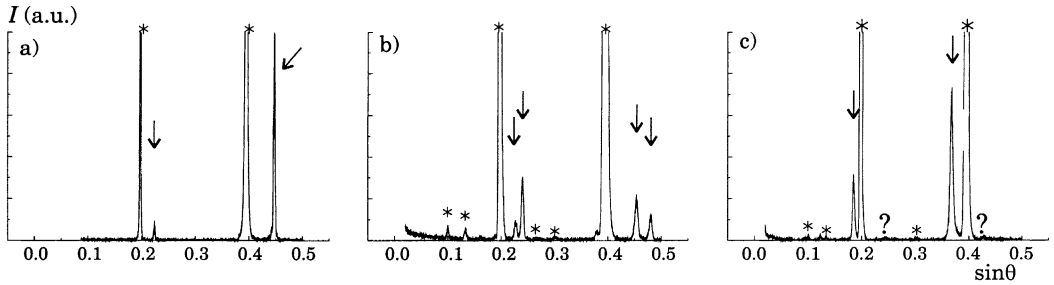

Fig. 2. XRD θ–2θ scans of (a) $SrCuO_2$, (b) bi-layer of $CaCuO_2$ and $Sr_{0.7}Ca_{0.3}CuO_2$, and (c) bi-layer $BaCuO_2$ and $SrCuO_2$, all deposited on $SrTiO_3$. Arrows indicate film peaks, * indicate peaks originating from the substrate. Some very small peaks were found, marked with ? in (c), corresponding to an unidentified phase or superstructure.

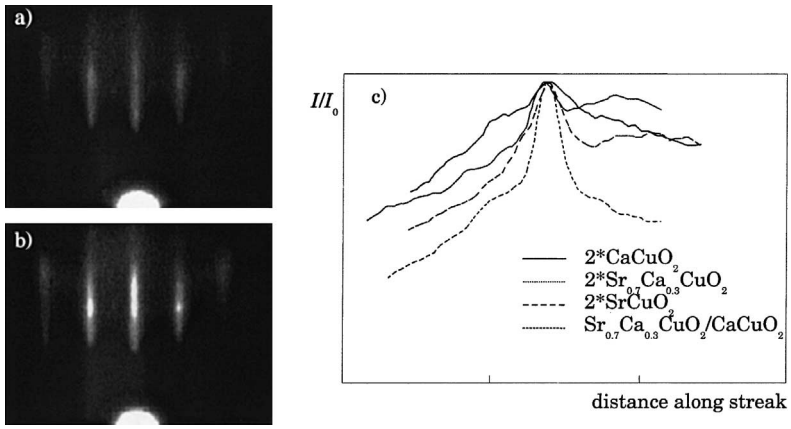

Fig. 3. Typical RHEED patterns after deposition of (a) a BCO block and (b) a (Sr,Ca)CO block. The profile along the 'specular' streak as a function of the composition of the latter is given in (c).

BCO/SCCO/CCO, respectively, is given. In all cases the deposition temperature was kept at 575°C with an oxygen pressure of 30 Pa. Apparently, the specular reflection has a sharper profile, indicating a smoother surface when the in-plane lattice constant of the composition approaches the lattice constant of $SrTiO_3$.

Examples of the intensity of the specular reflection recorded during interval deposition of these layers are given in Fig. 4. Fig. 4(a) (an enlargement of Fig. 4(b)), shows RHEED intensity variations during the deposition of a double BCO block in one interval, as seen from a sharp drop in intensity, followed by two single blocks of SCO.

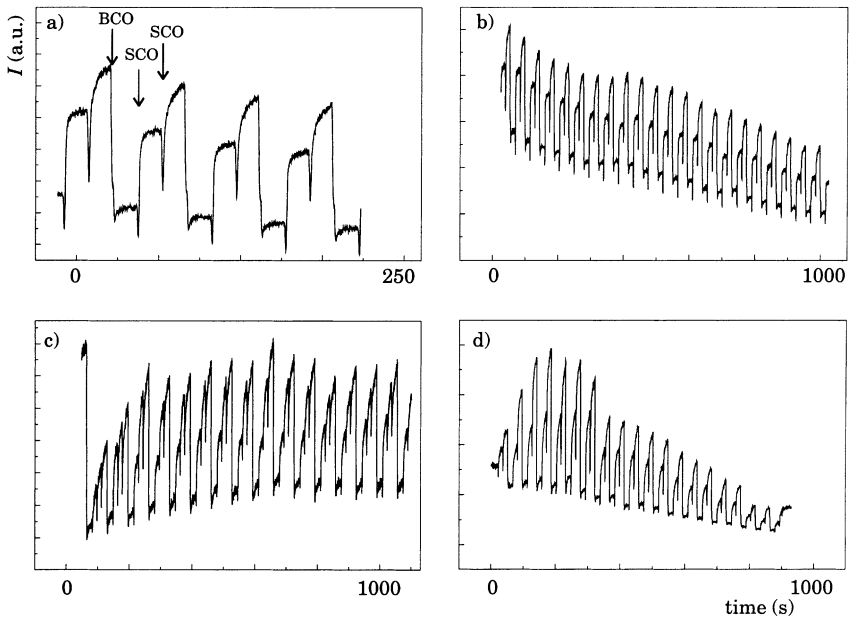

Fig. 4. Intensity of the specular reflection during deposition of (a) and (b) $[2BaCuO_2/2SrCuO_2]_{30}$, (c) $[2BaCuO_2/3Sr_{0.7}Ca_{0.3}CuO_2]_{30}$ and (d) $[2BaCuO_2/2CaCuO_2]_{20}$.

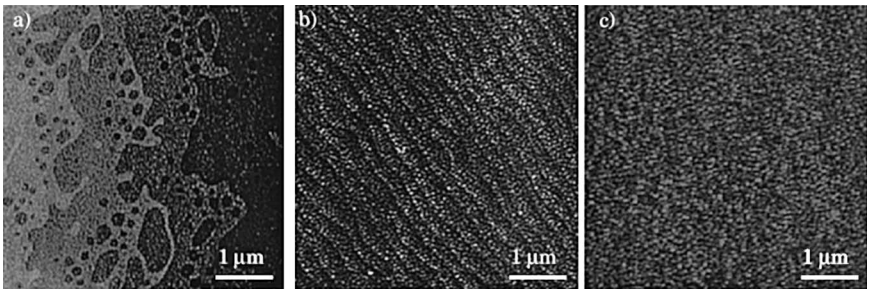

Fig. 5. Surface morphology as seen with AFM of (a) $(2BCO/2SCO)_{25}$ superlattice, (b) $(2BCO/2SCCO)_{25}$ and (c) $(2BCO/2CCO)_{25}$.

Each deposited block causes initially a drop, followed by a rise of the intensity. This type of oscillations are typical for the interval deposition method. For the SCO containing films, a reasonably constant amplitude of the intensity oscillations is observed, see Fig. 4(b) and (c), where films have been deposited with compositions 2BCO/2SCO and 2BCO/3SCO, respectively. This indicates a smooth surface during the deposition of 22 unit cells. This in contrast to the decrease of the intensity after deposition of a certain thickness ($\sim$17 BCO/CCO blocks) of films containing only Ca and Ba, see Fig. 4(d). This difference can be attributed to the larger in-plane lattice mismatch between BCO and CCO tetragonal structures, causing stress and subsequent release of this stress for thicker layers, forming a rougher surface.

Ex situ AFM shows that in case of the SCO/SCCO containing films almost complete suppression of island growth has been achieved, see Fig. 5(a) and (b). The initial terrace morphology of the substrate surface is still visible, with height differences originated from the $SrTiO_3$ unit-cell steps, even after the deposition of a 40 nm thick film. On the terraces, the morphology consists of small islands. In Fig. 5(a) an interesting feature can be seen. In this case the miscut angle of the $SrTiO_3$ substrate was very low ($<0.05°$) resulting using our chemical treatment in one unit-cell deep circular holes on the wide terraces [85]. After subsequent deposition of (2SCO/2BCO), still this unique imprint of the underlying substrate is visible, a strong evidence for layer-by-layer growth. It means that the constantly high-RHEED intensity is *not* due to a step-flow type of growth.

As seen in Fig. 5(c), the imprint of the substrate morphology is absent in the case of CCO containing films. However, as expected from RHEED analysis, the films are still reasonably smooth, which was also confirmed by X-ray reflectivity measurements. Note that the observed morphology of all these surfaces is expected to be affected by interaction with air (humidity). [3]

The θ–2θ scans of these artificial superstructures show clear satellite peaks, indicated with arrows, see Fig. 6. The positions of these satellite peaks were used to further calibrate the deposition rate of each constituent.

When the deposition rate for BCO was derived from the longer RHEED intensity oscillation period, see Fig. 1(c), the resulting films gave a superlattice period, which could not be fitted by simply adding the expected thickness of each constituent block. For example, Fig. 6(a) shows superlattice peaks up to high order, indicative for a high-quality superstructure. These satellite peaks are centered on the average peak located near the substrate peaks (sometimes they are merged). However, the measured $\Lambda = 3.83$ nm, determined using Eq. (1), does not correspond to the originally intended $4 + 2$ superlattice ($\Lambda \sim 2.2$ nm). The origin of this discrepancy will become clear from the HREM analysis, see below.

Reconsidering the deposition rate for BCO and taking the RHEED intensity oscillation period observed during deposition of the first few

[3] The alkaline earth (II) elements react easily with H_2O and CO_2 from the ambient.

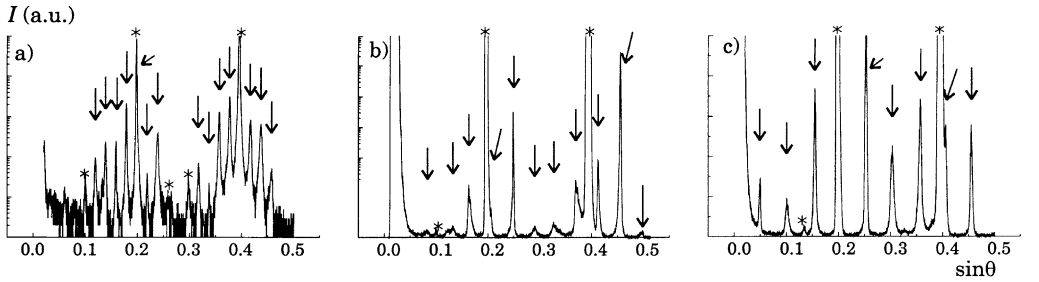

Fig. 6. θ–2θ scans of (a) BCO?/SCO? ($\Lambda \sim 3.8$ nm, i.e., corresponds *not* to 2BCO/4SCO), (b) 2BCO/2CCO/SCCO ($\Lambda \sim 1.803$ nm) and (c) BCO_2/CCO_2 ($\Lambda \sim 1.52$ nm). The (0 0 l) reflections of the films are indicated with arrows, peaks corresponding to the substrate are indicated with an asterisk.

monolayers, see Fig. 1(c), we obtained superstructures for which examples of the θ–2θ scans are shown in Fig. 6(b) and (c). The small width and the correct positions of the satellite peaks, according to Eq. (1), indicate a high quality of the superstructures. The satellite peaks correspond to superlattice periods that are much closer to the expected ones then in the case of Fig. 6(a).

If the exact number of laser shots that correspond to each constituent layer deviates from an integer, see Eq. (2), due to small errors in the estimate for the deposition rate or intermixing, the satellite peaks will broaden or even splitting can occur. The difference between a film with non-integer values for n_i see Fig. 6(b) and one with integer n_i, see Fig. 6(c), is exemplified: The former clearly shows broadening of the peaks located in between the average lattice peaks (which are located near the substrate peaks), whereas in the latter case, all the film peaks have the same width, indicative of a high-quality superlattice.

For 2SCO\2BCO and 2CCO\2BCO films, ω–2θ plots of the (0 1 3) peak are given in Fig. 7(a) and (b), respectively. The FWHM values for both films are of the same order, close to the value for instrumental broadening, although the latter film displays a little more spread in orientation, which could also be concluded from the RHEED measurements during deposition. These values are somewhat higher than those reported by Aruta et al. [86] or comparable [87].

The full data set of reflections collected for some of the films is indexed by a unit cell with a c-axis value corresponding to the superlattice period mentioned above. In addition, as expected, the in-plane lattice constants are close to the ones of the

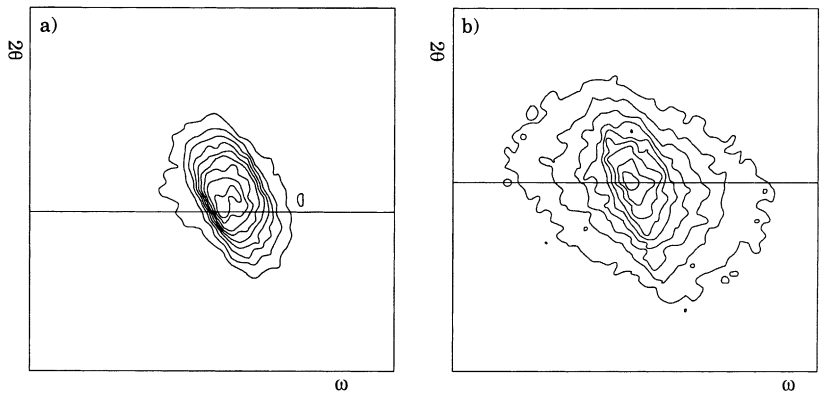

Fig. 7. ω–2θ plots of the superstructures (each contour represents a decrease of 10% of the maximum intensity starting from the peak value): (a) 2SCO/2BCO $(0\,\bar{1}\,3)$ $d\omega = d2\theta = 1.978°$; $2\theta(x_0) = 26.48°$; $\omega(y_0) = -2.34°$; FWHM $\sim 0.3°$; (b) 2CCO/2BCO $(0\,\bar{1}\,3)$ $d\omega = d2\theta = 1.978°$; $2\theta(x_0) = 27.07°$; $\omega(y_0) = 2.31°$; FWHM $\sim 0.35°$.

substrates. Refinement of the data set, using a model structure and treating the structure as a single crystal, did not lead to a conclusive result yet. From HREM, however, a better understanding of the microstructure can be obtained.

The superlattice periods derived for different compositions are given in Table 1. The values found are systematically larger than the ones expected (from simple summation of the thickness of the individual blocks, using the values found in Fig. 2). Note that the deviations are much smaller than in the case when wrong estimated deposition rates were used. By assuming a larger value than 0.42 nm (i.e., 0.44 nm) for the BCO blocks, a better fit to the measured values is obtained, similar to the observations of Balestrino et al. [67]. The nature of these deviations has been studied in more detail by HREM.

Fig. 8(a) shows an HREM overview of the hetero-structure as previously studied with XRD in Fig. 2(a). The top of the hetero-structure contains a protective $SrTiO_3$ layer. The dark layers, 20 in total, are SCO, and the lighter layers, also 20, are BCO. Fig. 8(b) shows a HREM image recorded near the top $SrTiO_3$ buffer layer. The BCO layers clearly have a periodicity that differs from the expected 'perovskite' spacing. The zig-zag contrast in the closely spaced double rows resembles the contrast of superconducting $(La,Ba)_2CuO_{4-\delta}$, were Ba layers are present and are shifted by $(1/2, 1/2)$ in the (a, b) plane, with respect to each other. The periodicity in the central row is clearly shifted by $(1/2)a_0$ after crossing the double row, as indicated by arrows in Fig. 8(b). The lattice parameter of the Ba block along the c-axis measured on the image is 1.32–1.36 nm.

All these features combined let us conclude that the BCO layers in these samples actually consist of Ba_2CuO_x. Others have observed similar structural features in SCO films [88]. We observed mostly two unit-cells thick layers of Ba_2CuO_x, with a total thickness of 2.72 nm. The observed periodicity in the image, three unit cells of SCO and two unit cells of Ba_2CuO_x, yields a total thickness of about 3.8 nm. Locally we observe regions with layers of two or four unit cells of SCO. It is interesting to note that the incorporation of Ba double layers results in a shift of the Cu sublattice, observed as a $(1/2)a_0$ shift. In the case of $1/2$ unit cell of Ba_2CuO_x this would result in a shift of the Cu sublattice in consecutive SCO layers. Also steps in the Ba_2CuO_x layer with heights of $1/2$ unit cell would induce this shift. However, such steps are rarely observed; all the SCO layers are aligned, as indicated with the vertical line in Fig. 8(b).

The contrast in the BCO layers could be matched with simulated images of Ba_2CuO_x for a defocus of -20 nm and thickness of 2 nm. The ratio of a/c for $SrCuO_2$ is 1.03 and the ratio for the Ba_2CuO_x is 3.97. Fig. 8(b) shows the positions of Ba (white circles) according to a model for the Ba_2CuO_x.

Fig. 9(a) shows a selected area electron diffraction (SAED) pattern. An enlargement around the

Table 1
Superlattice periods, using Eq. (1) for different compositions (nm)

	Expected values	Measured values	Literature
A: $BaCuO_2$	–	0.421	0.420 [67]
B: $SrCuO_2$	–	0.345	0.34 [24]; 0.346 [25]
C: $SrCaCuO_2$	–	0.338	0.340 [63]
D: $CaCuO_2$	–	0.321	0.316–0.321 [26]
2A + 2B	1.53 (0.383)	1.57–1.58	1.57 [68]
2A + 3B	1.875 (0.375)	1.91 (0.384)	1.92 [68]
2A + 4B	2.22 (0.370)	2.25 (0.379)	
2A + 2C	1.52 (0.379)	1.55–1.57	
2A + 3C	1.85 (0.371)	1.90	
2A + 2D	1.48 (0.370)	1.51–1.54 (0.376–0.382)	1.51 [87]
2A + 3D	1.80 (0.360)		1.82 [87]
2A + C + D	1.50 (0.374)	1.53	
2A + C + D + C	1.84 (0.367)	1.85 (0.368)	

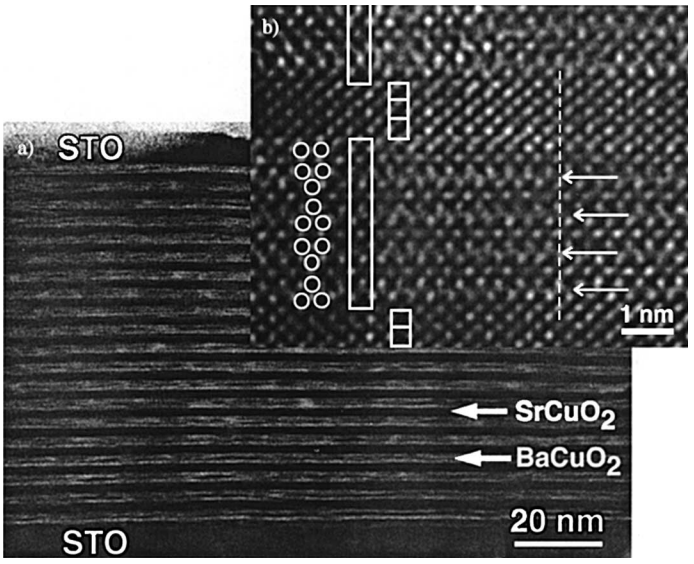

Fig. 8. (a) Overview TEM image of a SCO/BCO superlattice based on an incorrect deposition rate estimate for the $BaCuO_2$ layers, the white contrast corresponds to BCO, (b) HREM image of the same film, the white circles indicate the positions of the Ba ions in the Ba_2CuO_x model.

(0 0 4) reflection is given in Fig. 9(b). The superlattice periodicity obtained from this diffraction pattern is 3.54–3.56 nm. Faint spots are present near the basic perovskite spots as indicated by the upper arrow. The lower arrow indicates the perovskite structure. This faint spot is rather elongated and it represents a periodicity ranging from 0.358 to 0.362 nm belonging to the basic $ACuO_2$ building block.

Apart from the highly ordered regions in the films, we also observed that the BCO layer suffered from amorphization, as seen in Fig. 10(a). This clearly illustrates the instability of the BCO structure as compared to the SCO. Possibly due to

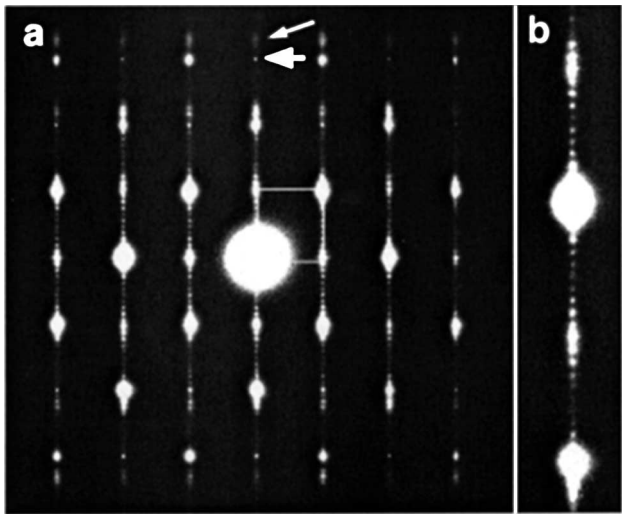

Fig. 9. (a) SAED pattern of the structure as given in Fig. 8 and (b) a closeup near the (4 0 0) reflection.

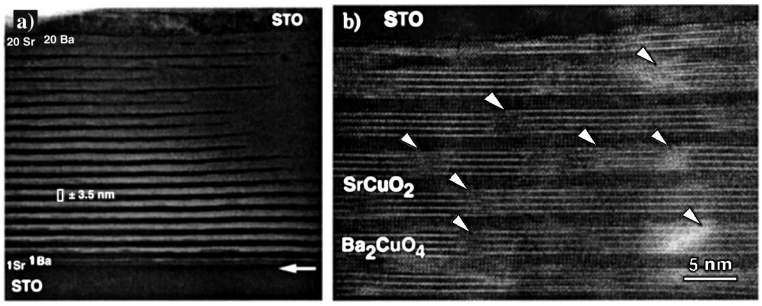

Fig. 10. (a) Amorphization of the BCO layers during TEM preparation and (b) shift of the unit cells (steps), indicated by arrows.

local deviations of the deposition rate, planar defects were also found, see Fig. 10(b). It is clear that the BCO layers contain steps as can be seen from the discontinuity of the white contrast lines. Steps in the BCO layers are indicated with arrows.

These observations explain the formerly unexpected superlattice (based on the deposition sequence) value found with XRD in Fig. 6(c) (which corresponds to two Ba_2CuO_x blocks and three SCO blocks) and point to the need to reconsider the deposition rate calibration in the case of BCO. This also might explain the change in the periodicity of the RHEED intensity oscillations seen in Fig. 1(d), although this was not clearly confirmed by XRD (Fig. 2(c)).

Fig. 11(a) shows a superlattice structure deposited after recalibration of the deposition rate of BCO, see also Fig. 12(c). The HREM image was

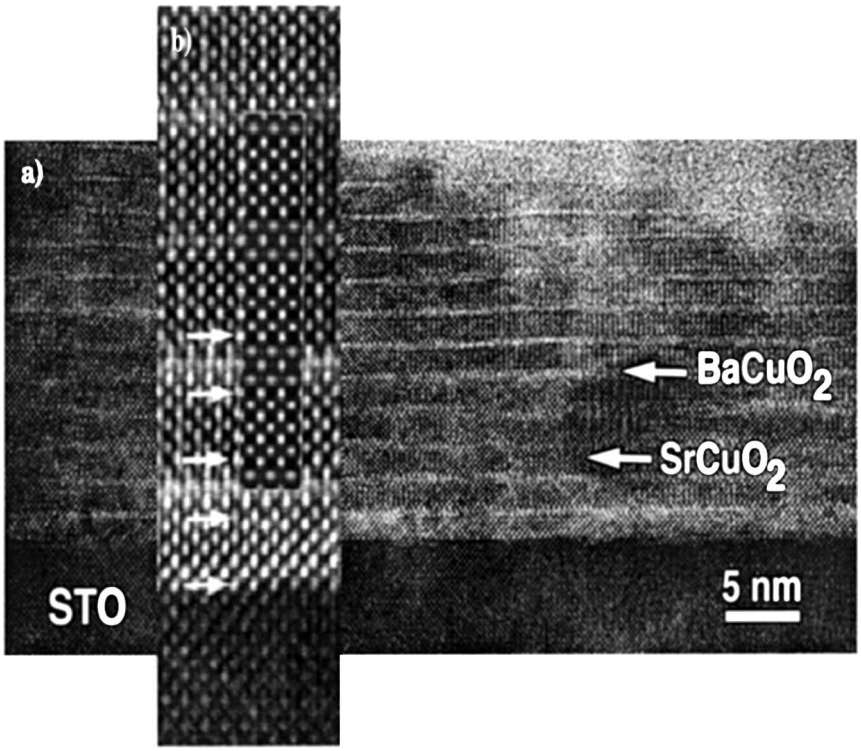

Fig. 11. (a) HREM image of a 3SCCO/2BCO structure, (b) enlargement; the arrows indicate the copper oxide planes.

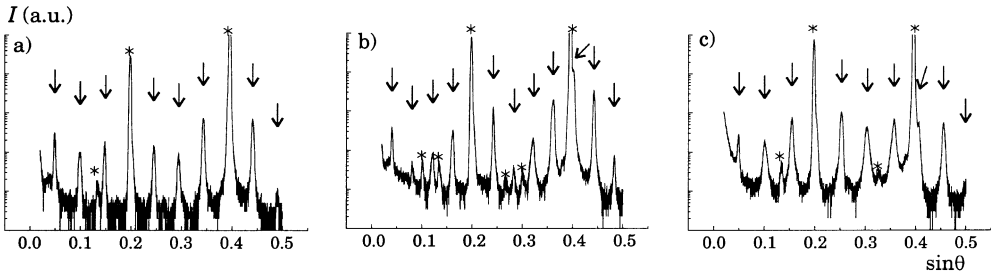

Fig. 12. θ–2θ scans of (a) 2BCO/2SCO ($\Lambda \sim 1.57$ nm), (b) 2BCO/3SCO ($\Lambda \sim 1.91$ nm) and 2BCO/2CCO ($\Lambda \sim 1.52$ nm) superlattices. The (0 0 l) reflections of the films are indicated with arrows, and the peaks corresponding to the substrate are indicated with an asterisk.

taken close to the STO substrate. The superlattice in this region is nearly perfect. Fig. 11(b) is an enlargement of Fig. 11(a) from which the noise due to an amorphous overlayer has been removed. The image shows only contrast originated from the perovskite structure. The lattice spacing for each layer (measured from the images with calibration on STO) is 0.408–0.425 nm for BCO and 0.343–0.363 nm for SCCO. The superperiod measured from computer diffractograms obtained from image of Fig. 11(b) is 1.90–2.04 nm.

Here, we observe that BCO is indeed present in the infinite-layer structure. In the image of Fig. 11(b), taken at defocus of -70 nm with a thickness of about 2 nm, the contrast can be interpreted as Cu represented by white dots. Here, the order of deposition has been SrO/SCCO/BCO on $SrTiO_3$. If we look in detail to the layer stacking, as starting from the inside of the film towards the substrate, we count seven layers from the CuO layer, which is the interface between the first BCO and the SCCO. This corresponds to three unit cells of SCCO in the first layer growing on SrO terminated STO, seen to exhibit a darker contrast then the superlattice structure. The ratio between the Sr and Ba unit cell is 1.16 as determined from the maxims of a line plot from Fig. 11(b). Here, image simulations are based on a model where Cu layers are fully oxidized in, both, the SCCO layer as well as in the BCO layers. The Ba layers were assumed to contain no oxygen. Possibly even better matching could be achieved by varying the O distribution.

Fig. 13(a) shows a diffraction pattern with the superstructure reflections. An enlargement around the (0 0 4) reflection is given in Fig. 13(b). The superstructure spots are streaked along the growth direction, impeding a precise superstructure period determination. The measured values range between 1.85 and 2.04 nm. Comparing the c-axis values with the values obtained by XRD measurements, we conclude that the superlattice periods are similar, although somewhat larger than the expected value [89]. However, HREM did not confirm convincingly that the observed enlargement can be explained by an expansion of the BCO block in the c-direction solely.

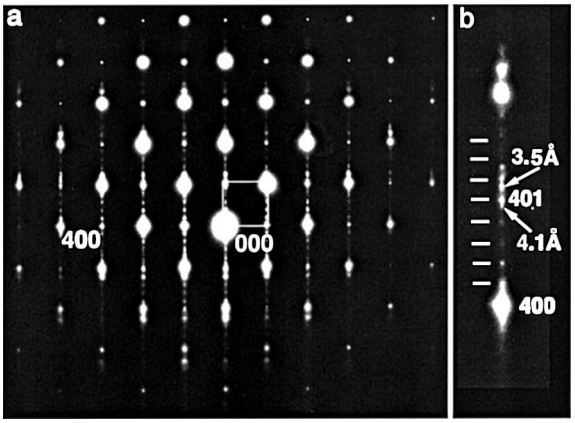

Fig. 13. (a) SAED pattern of the structure as in Fig. 11 and (b) a closeup near the (4 0 0) reflection.

In this sample, deviations from the perfect structure were also found. Fig. 14 shows a region of the superlattice that is highly defective. Large substrate steps are present, resulting in a highly defective superlattice. This stresses the importance of a well-prepared substrate surface.

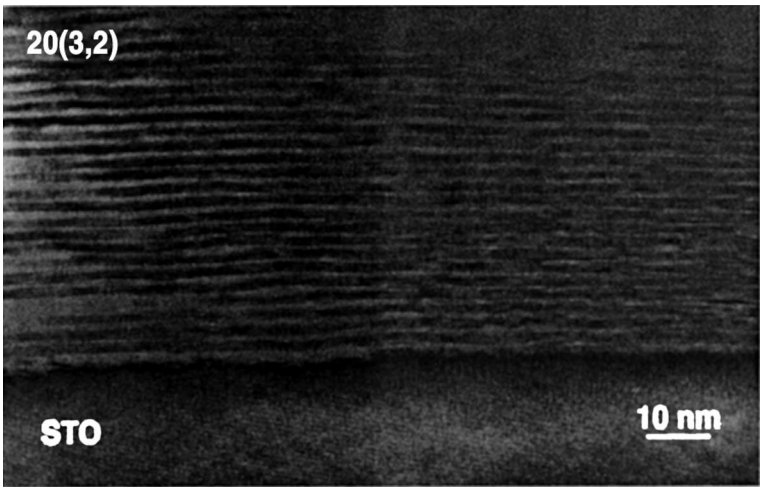

Fig. 14. HREM image near a highly defective region of the substrate surface.

Finally, the electrical properties of the superlattices were measured and the following behavior was observed. SCO/BCO films cooled down after deposition in a low oxygen ambient (i.e. the deposition pressure), show a high resistance at room temperature, which exponentially increases with decreasing temperature, see Fig. 15(a) (curve 1). When similar films were cooled down in a high pressure ambient (>200 mbar) to roughly 400°C and, subsequently, quenched to room temperature, [4] a significantly lower resistance was observed (curve 2). Also initially 'low pressure' cooled films which were brought to the deposition temperature again in a tube oven while flushing with pure oxygen and subsequently quenched to room temperature showed a lower resistance as well (curve 3). Yet, upon cooling in liquid He they showed always a 'semiconducting' behavior.

The observations described above indicate the possibility to control the oxygen content of the films and, thereby, the conducting properties. However, more research has to be done, to obtain the optimal settings for every film composition. For example, we have assumed the aforementioned 'quench' procedure to be optimal for all other films, which need not be the case.

A series of five films deposited at 575°C and 31 Pa but with different compositions in general showed a decrease in resistance with an increase in CCO layers, see Fig. 15(b) (curves 2–6). [5] Here, a film, which contained no Sr at all (curve 1) displays 'semiconducting' behavior, in contrast with other observations for films with a similar composition, indicating the difficulty of controlling the conducting properties.

Metal-like behavior and even superconducting transitions to zero resistance were only observed for films with at least one CCO layer, see Fig. 15(b) (curves 4–6), deposited at temperature around 575°C with an oxygen pressure >20 Pa. Note, that the temperature/pressure window for good quality CCO containing films, is small, as determined from the RHEED measurements. The

[4] Here, quenching to room temperature was done by removing the sample holder from the deposition chamber and subsequently detaching the sample from the heater block as fast as possible.

[5] The measurements presented in this figure are performed by using sputter deposited gold contact pads in order to obtain good conducting contacts, whereas the results given in the other figures were done by directly bonding Al wires onto the film. Due to the difference in contact area, the resistance values are hard to compare.

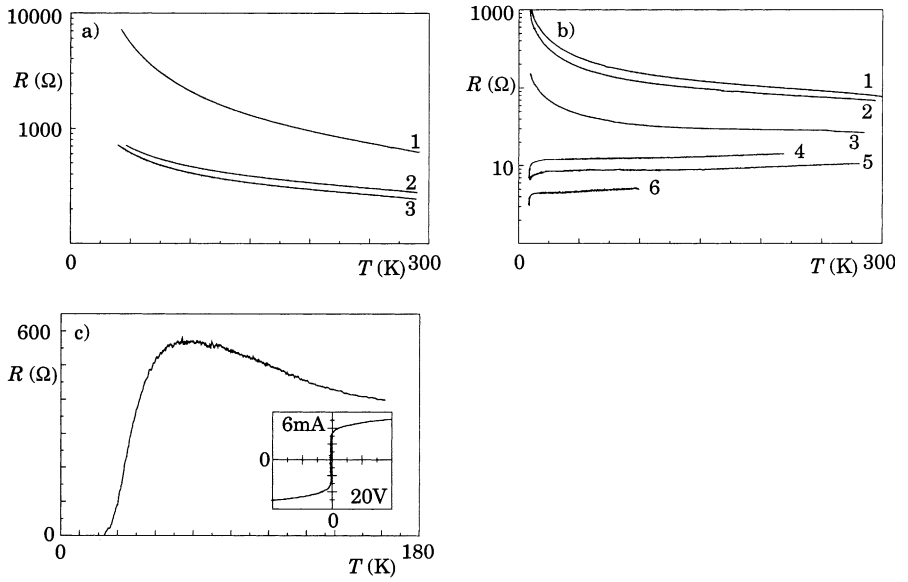

Fig. 15. Resistance versus temperature of (a) 2SCO/2BCO – 1. after cooling down at low pressure, 2. after cooling down at high pressure, 3. same as 1 plus annealing in tube oven in flow of oxygen; (b) 1. 2CCO/2BCO, 2. 2SCO/2BCO, 3. SCCO/2BCO, 4. SCCO/CCO/2BCO, 5. SCCO/CCO/2BCO, 6. 2SCCO/CCO/2BCO, all deposited at 575°C and 31 Pa and (c) 2CCO/2BCO deposited at 575°C and 20 Pa; here, the inset is the *I–V* curve measured at ~8 K.

highest $T_{c,onset}$ was ~50 K and $T_{c,zero}$ ~ 12 K, see Fig. 15(c). This film showed an increase in resistance before getting into the superconducting state. To confirm superconductivity, we performed an *I–V* characterization at ~8 K, see the inset of Fig. 15(c).

4. Conclusions

We have shown that PLD in combination with an in situ analysis technique makes fabrication of superlattice structures of oxide materials down to the atomic level feasible. RHEED proved to be a useful tool to estimate the deposition rate of constituent materials, through the intensity oscillations. However, careful analysis showed that one cannot always rely on the observation of intensity oscillations, the period of which may correspond to unexpected amounts deposited, e.g., in the case of BCO.

The choice of $SrTiO_3$ as the substrate material proved to be valid for the stabilization of the infinite-layer structure. The deposition temperature and oxygen pressure are far below the normally used conditions to stabilize this structure in the bulk phase. In addition, from AFM observations it became clear that the high quality of the substrate surface ensured a perfect template for epitaxy. HREM analysis clearly shows that the lattice of the film material, here mostly compressed in-plane, is determined by the lattice parameters of the substrate. Therefore, other substrate materials with similar surface properties might yield different conducting properties of the films and are currently being investigated.

We proved that the interval deposition method indeed suppresses the formation of larger islands or a multi-level growth front, almost irrespective of the deposition conditions, with the degree of suppression depending on the constituents deposited. When, from the aspect of thermodynamic stability, another (layered) phase is formed, interval deposition cannot prevent this. Even in the case of 3D nucleation (e.g., release of stress) the method can still be useful, since the formation of large islands is prevented, although one of the requirements for the use of interval deposition was

assumed to be 2D nucleation. This might explain the success achieved with the CCO/BCO films, for limited thickness, where stress is expected to be considerable.

The structural analysis with XRD and HREM of the superlattices indicates first of all a high-quality structure, in both the overall crystallinity as well as in the imposed periodicity along the *c*-axis. Furthermore, the right estimate for the deposition rate per constituent was confirmed by the period of the superlattices. A systematic deviation turned out to be caused by the compressive stress in the film. To our knowledge, the HREM images of Ba containing infinite-layer thin films are the first reported so far.

The results presented here indicate that superconductivity is related to defect structures responsible for charge-carrier doping of the copper oxide planes. The most perfect structures, e.g., $SrCuO_2$/$BaCuO_2$ superlattices, were never superconducting, whereas for the superconducting films, defects are expected to be present, although we did not find a systematic proof. It is clear that almost true layer-by-layer growth does not necessarily lead to good superconducting properties, i.e., high-T_cs.

The difference in A-cation size for successive layers in a superlattice structure is found to influence the growth behavior. First, the Sr and Ba containing structures can be deposited in a much wider temperature and pressure window (500–600°C and >3 Pa), compared to structures with only Ca and Ba (550°C and >20 Pa). Secondly, the Ca and Ba containing structure were found to grow in a layer-by-layer fashion up to a certain thickness, which is explained by the release of stress beyond that thickness.

The goal to achieve atomically engineered layered oxides and interfaces, enabling to systematically investigate the relation between microstructure and macroscopic properties has been made possible with this technique-interval deposition with high-pressure RHEED.

Acknowledgements

The work was supported by the Dutch foundation of fundamental research of matter FOM.

References

[1] C.N.R. Rao, J. Gopalakrishnan, New Directions in Solid State Chemistry, second ed., Cambridge University Press, Cambridge, UK, 1997 (chapter 3).
[2] J.-M. Triscone, Ø. Fischer, O. Brunner, L. Antognazza, A.D. Kent, Phys. Rev. Lett. 64 (1990) 804.
[3] Q. Li, X.X. Xi, X.D. Wu, A. Inam, S. Vadlamannati, W.L. McLean, Phys. Rev. Lett. 64 (1990) 3086.
[4] T. Satoh, T. Tereshima, K. Shimura, Z. Hiroi, Y. Bando, Physica C 185–189 (1991) 2033.
[5] Y. Bando, T. Terashima, K. Shimura, T. Sato, Y. Matsuda, S. Komiyama, K. Kamigaki, H. Terauchi, Physica C 185–189 (1991) 204.
[6] O. Eibl, Mat. Sci. Eng. B 10 (1991) 305.
[7] D.P. Norton, D.H. Lowdnes, S.J. Pennycook, J.D. Budai, Phys. Rev. Lett. 67 (1991) 1358.
[8] H. Tabata, T. Kawai, S. Kawai, Phys. Rev. Lett. 70 (1993) 2633.
[9] A. Gupta, R. Gross, E. Olsson, A. Segmüller, G. Koren, C.C. Tsuei, Phys. Rev. Lett. 64 (1990) 3191.
[10] T. Kawai, T. Matsumoto, M. Kanai, H. Tabata, K. Horiuchi, S. Kawai, Physica C 185–189 (1991) 198.
[11] I. Bozovic, J.N. Eckstein, Proceedings 10th Anniversary HTS Workshop on Physics, Materials, and Applications, Houston, TX, World Science, Singapore, 1996, p. 103.
[12] A. Chaiken, M.A. Wall, R.H. Howell, I. Bozovic, J.N. Eckstein, G.F. Virshup, J. Mater. Res. 11 (1996) 1609.
[13] M. Laguës, X.M. Xie, H. Tebbji, X.Z. Xu, V. Mairet, C. Hatterer, C.F. Beuran, C. Deville-Cavellin, Science 262 (1993) 1850.
[14] T. Kawai, Y. Egami, H. Tabata, S. Kawai, Nature 349 (1991) 200.
[15] R. Tsuchiya, M. Kawasaki, H. Kubota, J. Nischino, H. Sato, H. Akoh, H. Koinuma, Appl. Phys. Lett. 71 (1997) 1570.
[16] S.P. Benz, C.D. Reintsema, R.H. Ono, J.N. Eckstein, I. Bozovic, G.F. Virshup, IEEE Trans. Appl. Supercond. 5 (1995) 2915.
[17] J.N. Eckstein, I. Bozovic, G.F. Virshup, IEEE Trans. Appl. Supercond. 5 (1995) 1680.
[18] M. Marezio, C. Chaillout, Materials and Crystallographic Aspects of HT_c-superconductivity, Kluwer Academic Publishers, Dordrecht, 1994, p. 3.
[19] B. Raveau, High-T_c Superconductivity: Ten Years After the Discovery, NATO ASI Series E 343, Kluwer Academic Publishers, Dordrecht, 1996, p. 109.
[20] T. Siegrist, S.M. Zahurak, D.W. Murphy, R.S. Roth, Nature 334 (1988) 231.
[21] M. Kanai, T. Kawai, S. Kawai, Appl. Phys. Lett. 58 (1991) 771.
[22] C. Niu, C.M. Lieber, J. Am. Chem. Soc. 114 (1992) 3570.
[23] D.P. Norton, B.C. Chakoumakos, J.D. Budai, D.H. Lowndes, Appl. Phys. Lett. 62 (1993) 1679.
[24] S. Gonda, H. Nagata, M. Kawasaki, M. Yoshimoto, H. Koinuma, Physica C 216 (1993) 160.

[25] A. Gupta, M.Y. Chern, B.W. Hussey, Physica C 209 (1993) 175.
[26] A. Gupta, B.W. Hussey, T.M. Shaw, A.M. Guloy, M.Y. Chern, R.F. Saraf, B.A. Scott, Solid State Chem. 112 (1994) 113.
[27] G. Balestrino, R. Desfeux, S. Martellucci, A. Paoletti, G. Petrocelli, A. Tebano, B. Mercey, M. Hervieu, J. Mater. Chem. 5 (1995) 1879.
[28] I. Kawayama, M. Kanai, T. Kawai, Jpn. J. Appl. Phys. 35 (1996) L926.
[29] I. Yazawa, N. Terada, K. Matsutani, R. Sugise, M. Jo, H. Ihara, Jpn. J. Appl. Phys. 29 (1990) L566.
[30] N. Terada, G. Zouganelis, M. Jo, M. Hirabayashi, K. Kaneko, H. Ihara, Physica C 185–189 (1991) 2019.
[31] Y. Terashima, R. Sato, S. Takeno, S. Nakamura, T. Miura, Jpn. J. Appl. Phys. 32 (1993) L48.
[32] S. Nagai, H. Tanaka, N. Fujimura, T. Ito, J. Appl. Phys. 77 (1995) 3805.
[33] H. Adachi, M. Sakai, T. Satoh, K. Setsune, Physica C 244 (1995) 282.
[34] X. Li, M. Kanai, T. Kawai, S. Kawai, Jpn. J. Appl. Phys. 31 (1992) L217.
[35] M. Kawai, Z.-Y. Liu, T. Hanada, M. Katayama, M. Aono, C.F. McConville, Appl. Surf. Sci. 82 (1994) 487.
[36] H. Osagawara, T. Sakuma, M. Tsukakoshi, M. Kawai, Thin Solid Films 281–282 (1996) 120.
[37] M. Yoshimoto, H. Nagata, S. Gonda, J.P. Gong, H. Ohkubo, H. Koinuma, Physica C 190 (1991) 43.
[38] M. Yoshimoto, H. Nagata, J. Gong, H. Ohkubo, H. Koinuma, Physica C 185–189 (1991) 2085.
[39] A. Brazdeikis, A.S. Flodström, Appl. Surf. Sci. 107 (1996) 95.
[40] K. Kobayashi, Y. Ishihara, S. Matsushima, G. Okada, Jpn. J. Appl. Phys. 30 (1991) L1931.
[41] G. Wen, H. Yakabe, A. Kumu, Y. Shiohara, N. Koshizuka, S. Tanaka, Physica C 228 (1994) 279.
[42] M.G. Smith, A. Manthiram, J. Zhou, J.B. Goodenough, J.T. Markert, Nature 351 (1991) 549.
[43] G. Er, Y. Miyamoto, F. Kanamura, S. Kikkawa, Physica C 181 (1991) 206.
[44] C.L. Wooten, O. Beom-hoan, J.T. Markert, M.G. Smith, A. Manthiram, J. Zhou, J.B. Goodenough, Physica C 192 (1992) 13.
[45] W. Korczak, M. Perroux, P. Strobel, Physica C 193 (1992) 303.
[46] N. Ikeda, Z. Hiroi, M. Azuma, M. Takano, Y. Bando, Physica C 210 (1993) 367.
[47] C. Niu, C.M. Lieber, Appl. Phys. Lett. 61 (1992) 1712.
[48] M.Y. Chern, A. Gupta, B.W. Hussey, Appl. Phys. Lett. 60 (1992) 3045.
[49] H. Adachi, T. Satoh, Y. Ichikawa, K. Setsune, K. Wase, Physica C 196 (1992) 14.
[50] N. Sugii, K. Matsuura, K. Kubo, K. Yamamoto, M. Ichikawa, H. Yamauchi, J. Appl. Phys. 74 (1993) 4047.
[51] E. Koller, L. Miéville, L. Fàbrega, J.-M. Triscone, Ø. Fischer, Physica C 235–240 (1994) 707.
[52] N. Sugii, M. Ichikawa, K. Kubo, T. Sakurai, K. Yamamoto, H. Yamauchi, Physica C 196 (1992) 129.
[53] M. Azuma, Z. Hiroi, M. Takano, Y. Bando, Y. Takeda, Nature 356 (1993) 775.
[54] Z. Hiroi, M. Takano, M. Azuma, Y. Takeda, Nature 364 (1993) 315.
[55] H. Zhang, Y.Y. Wang, H. Zhang, V.P. Dravid, L.D. Marks, P.D. Han, D.A. Payne, P.G. Radaelli, J.D. Jorgensen, Nature 379 (1994) 352.
[56] S. Adachi, H. Yamauchi, S. Tanaka, N. Môri, Physica C 212 (1993) 164.
[57] H. Shaked, Y. Shimakawa, B.A. Hunter, R.L. Hitterman, J.D. Jorgensen, P.D. Han, D.A. Payne, Phys. Rev. B 51 (1995) 11784.
[58] M. Laguës, C.F. Beuran, C. Deville, B. Eustache, P. Germain, C. Hatterer, V. Mairet, C. Partiot, X.M. Xie, X.Z. Xu, in: D. Pavuna, I. Bozovic (Eds.), Proceedings of the SPIE 2697, 1996, p. 192.
[59] R. Feenstra, X. Li, M. Kanai, T. Kawai, S. Kawai, J.D. Budai, E.C. Jones, Y.R. Sun, J.R. Thompson, S.J. Pennycook, D.K. Christen, Physica C 224 (1994) 300.
[60] R. Feenstra, J.D. Budai, D.K. Christen, T. Kawai, Appl. Phys. Lett. 66 (1995) 2283.
[61] M. Takano, Y. Takeda, H. Okada, M. Miyamoto, T. Kusaka, Physica C 159 (1989) 375.
[62] M. Takano, M. Azuma, Z. Hiroi, Y. Bando, Physica C 176 (1991) 441.
[63] D.P. Norton, J.D. Budai, D.H. Lowndes, B.C. Chakoumakos, Appl. Phys. Lett. 65 (1994) 2869.
[64] A. Tsukamoto, J.G. Wen, K. Nakanishi, K. Tanabe, Physica C 292 (1997) 17.
[65] G. Koster, G.J.H.M. Rijnders, D.H.A. Blank, H. Rogalla, Mat. Res. Soc. Symp. Proc. 502 (1998) 255.
[66] D.P. Norton, B.C. Chakoumakos, J.D. Budai, D.H. Lowndes, B.C. Sales, J.R. Thompson, D.K. Christen, Science 265 (1994) 2074.
[67] G. Balestrino, S. Martellucci, P.G. Medaglia, A. Paoletti, G. Petrocelli, Physica C 302 (1998) 78.
[68] D.P. Norton, B.C. Chakounakos, D.H. Lowndes, J.D. Budai, Appl. Surf. Sci. 96–98 (1996) 672.
[69] G. Balestrino, S. Martelucci, P.G. Medaglia, A. Paoletti, G. Petrocelli, A.A. Varlamov, Phys. Rev. B 58 (1998) R8925.
[70] J. Akimoto, K. Tokiwa, A. Iyo, H. Ihara, H. Hayakawa, Y. Gotoh, Y. Oosawa, Physica C 279 (1997) 181.
[71] R. Feenstra, J.D. Budai, D.K. Christen, T. Kawai, Appl. Phys. Lett. 67 (1995) 1310.
[72] J.L. Allen, B. Mercey, W. Prellier, J.F. Hamet, M. Hervieu, B. Raveau, Physica C 241 (1995) 158.
[73] M. Hervieu, B. Mercey, W. Prellier, J.L. Allen, J.-F. Hamet, B. Raveau, J. Mater. Chem. 6 (1996) 165.
[74] B. Raveau, M. Hervieu, C. Michel, Physica C 263 (1996) 151.
[75] K.-W. Chang, B.W. Wessels, W. Qian, V.P. Dravid, J.L. Schindler, C.R. Kannewurf, D.B. Studebaker, T.J. Marks, R. Feenstra, Physica C 303 (1998) 11.

[76] Y.Y. Xue, Y.Y. Sun, I. Rusakova, D.K. Ross, Z.L. Du, N.L. Wu, Y. Gao, L. Gao, B. Hickey, C.W. Chu, Physica C 294 (1998) 316.
[77] C.W. Chu, Y. Cao, Z.L. Du, L. Gao, K. Ross, I. Rusakova, Y.Y. Sun, N.L. Wu, Y.Y. Xue, Physica C 282 (1997) 57.
[78] G.J.H.M. Rijnders, G. Koster, D.H.A. Blank, H. Rogalla, Appl. Phys. Lett 70 (1997) 1888.
[79] M. Kawasaki, K. Takahashi, T. Maeda, R. Tsuchiya, M. Shinohara, O. Ishiyama, T. Yonezawa, M. Yoshimoto, H. Koinuma, Science 226 (1994) 1540.
[80] G. Koster, B.L. Kropman, G.J.H.M. Rijnders, D.H.A. Blank, H. Rogalla, Appl. Phys. Lett. 73 (1998) 2920.
[81] G. Koster, G.J.H.M. Rijnders, D.H.A. Blank, H. Rogalla, Appl. Phys. Lett. 74 (1999) 3729.
[82] E.E. Fullerton, I.K. Schuller, H. Vanderstraeten, Y. Bruynsraede, Phys. Rev. B 45 (1992) 9292.
[83] J. Karpinski, I. Mangelschots, H. Schwer, K. Conder, A. Morawski, T. Lada, A. Paszewin, Physica C 234–240 (1994) 917.
[84] T. Maeda, M. Yoshimoto, K. Shimozono, H. Koinuma, Physica C 247 (1995) 142.
[85] G. Koster, G. Rijnders, D.H.A. Blank, H. Rogalla, Physica C 339 (2000) 215.
[86] B. Aruta, G. Balestrino, S. Martelluci, A. Paoletti, G. Petrocelli, J. Appl. Phys. 81 (1997) 220.
[87] A. DelVecchio, L. Merenghi, L. DeCaro, L. Tapfer, C. Aruta, G. Petrocelli, G. Ballestrino, J. Appl. Phys. 82 (1997) 5465.
[88] N. Sugii, M. Ichikawa, K. Hayashi, K. Kubo, K. Yamamoto, H. Yamauchi, Physica C 213 (1993) 345.
[89] G. Koster, G.J.H.M. Rijnders, D.H.A. Blank, H. Rogalla, Mat. Res. Soc. Sym. Proc. 569 (1999) 35.